Comparative Study of Phase Change Material Characterization Methods

Maxime Thonon[1], Yasmine Lalau[2], Enghok Leang[3], Erwin Franquet[2], Gilles Fraisse[1], Stéphane Gibout[2], Laurent Zalewski[3]

[1] Univ. Savoie Mont Blanc, CNRS, LOCIE, 73000 Chambéry, France

[2] Universite de Pau et des Pays de l'Adour, E2S UPPA, LaTEP, Pau, France

[3] Laboratoire de Génie Civil et géo-Environnement, Université d'Artois, ULR 4515, F-62400 Béthune, France

Abstract

Modeling latent heat thermal energy storage systems is mostly achieved by implementing the enthalpy curve of the phase change material (PCM) into a numerical model. Then, the accuracy of the model depends on the accuracy of the enthalpy curve. The objective of this study is to compare the enthalpy curve obtained with four different characterization methods. Two methods are based on differential scanning calorimeter (DSC) experiments with dynamic and step modes. By modeling an experimental set-up, which contains a greater mass of PCM than with DSC, the two other methods use inverse methods to identify the analytical model describing the phase change process. Paraffin RT58, a PCM suitable for domestic hot water (DHW) storage, is selected for this study. Results highlight the same enthalpy difference for each method between 20°C and 65°C. Even if the end of the phase change process is described slightly differently for the two DSC methods than for the two inverse methods, results are mainly similar and all methods give a correct description of the phase change process. Conclusions are only relevant for the studied PCM, which does not undergo supercooling.

Keywords: PCM, Characterization, Enthalpy curve, DSC, Inverse method

Nomenclature

Latin letters

C_{eff}	Effective heat capacity, $\mathrm{J.kg^{-1}.K^{-1}}$
C_p	Specific heat capacity, $\mathrm{J.kg^{-1}.K^{-1}}$
f	Liquid fraction
H	Enthalpy, $\mathrm{J.kg^{-1}}$
L	Latent heat, $\mathrm{kJ.kg^{-1}}$
m	Mass, kg
T	Temperature, K
t	Time, s

Greek letters

Δt	Time step, s
ϵ	Coefficient of latent heat repartition
ϕ	Heat flux, W
λ	Thermal conductivity, $\mathrm{W.m^{-1}.K^{-1}}$
ρ	Density, $\mathrm{kg.m^{-3}}$
σ	Coefficient of analytical model

Subscripts

L	Liquid
PC	Phase change
S	Solid
Tot	Total

Exponent

Exp	Experimental

doi:10.18086/eurosun.2020.07.05 Available at http://proceedings.ises.org

Hx	**Heat exchanger**
Num	**Numerical**
PCM	**Phase change material**
$PMMA$	**Poly(methyl methacrylate)**
$Sens$	**Sensible heat**

1. Introduction

Latent heat thermal energy storage (LHTES) systems seem promising to store heat with a high energetic density, and PCM are already used in various applications (Sharma et al., 2009). A correct sizing of a LHTES system requires both an accurate modeling of the phase change process and an accurate identification of the PCM properties. As shown by (Dolado et al., 2012), a rather slight uncertainty on the phase change temperature leads to a high uncertainty on the heat exchange during charging and discharging process.

PCM characterization with DSC is the most common method to obtain both the PCM properties and the enthalpy curve describing the phase change process. Supercooling apart, the enthalpy curve of a PCM must be unique and only dependent on the temperature according to (Dumas et al., 2014). However, the heating rate and the mass of the PCM sample might influence the results as observed by (Lazaro et al., 2013).

The identification of PCM properties and the phase change dynamic might also be achieved by inverse method. An analytical formulation of the thermodynamic state of the PCM, depending only on the temperature, is used in a numerical model representing the experimental set-up. The parameters involved in the analytical model are then identified with an optimization algorithm to fit the numerical heat flux with the experimental, used as a reference. The inverse method might be performed on experimental results coming from DSC experiments (Franquet et al., 2012) or from a heat flux bench (Tittelein et al., 2015).

The PCM selected for this study is RT58, a paraffin manufactured by Rubitherm. This PCM is suitable for DHW storage with a phase change temperature around 58°C and no supercooling phenomenon. The objective of this study is to compare four PCM characterization methods. Two of them rely on DSC experiments, one with dynamic mode and the other with step mode. The two others characterization method are based on inverse methods with a global identification or an energy balance identification.

2. Differential scanning calorimeter characterization

2.1. Dynamic mode

PCM characterization by DSC with dynamic mode consists in monitoring the heat flux exchanged between a sample of few milligrams of PCM and its surrounding. Figure 1 illustrates the principle of DSC characterization with the dynamic mode for heating and cooling experiments. The enthalpy curve is obtained by plotting the exchanged heat in function of the temperature applied to the sample. As mentioned before, the heating and cooling rate might influence the results as the sample temperature is not exactly equal to the heat source temperature during the phase change. Indeed, the PCMs for LHTES are selected for their high thermal storage capacity, and most of them tend to have low thermal conductivity: that results in internal temperature gradient during their thermal characterisation. The sample temperature being measured on its external surface, this temperature will be overestimated during heating and underestimated during cooling. Thus, the true sample temperature should be enclosed by the heating and cooling curves. The challenge is then to find the appropriate temperature rate that minimize the difference between heating and cooling measurements. A low speed would minimize the sample thermal gradient but should not lead to an important signal-to-noise ratio that would increase the error in enthalpy variation estimation. One can note that it is impossible to determine for PCMs with high supercooling degree.

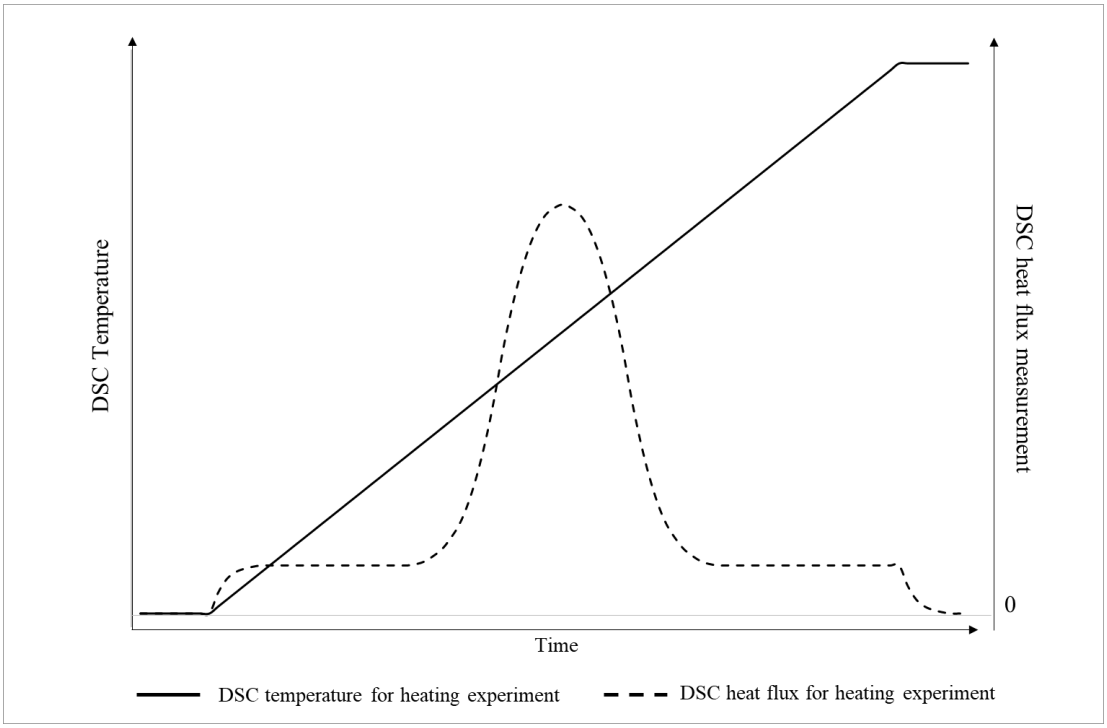

Fig. 1: Principe of DSC characterization with the dynamic mode

For RT58, this rate is reached for heating and cooling rate of 0.5 K.min^{-1}. Even if the difference between the heating and cooling curve is at its minimum for this rate, the two curves do not completely match one another. The average value between the enthalpy curve of heating and cooling is then selected to obtain the enthalpy curve of RT58 by DSC on dynamic mode.

2.2. Step mode

The DSC step mode consists of setting small temperatures step to heat the PCM sample, waiting for thermal equilibrium between each step identified by a signal returning to zero. Figure 2 illustrates the principle of DSC characterization with the step mode. The energy exchanged between two steps is monitored by plotting the flux along the temperature for each step, forming a peak which area is proportional to the heat absorbed by the sample. Then, the enthalpy curve may be built from this data by plotting the energy absorbed by the sample for each temperature step. Compared to the dynamic mode, the step mode overcomes the rate influence and is less dependent to the mass of the sample. However, the experimental characterization requires a longer duration as the thermal equilibrium has to be reached before applying the next temperature step. The temperature difference between two steps is also a parameter which might influence the results (Gibout et al., 2017). A too high temperature step leads to an inaccurate representation of the phase change process as the heat flux peak is not clearly identified. On the contrary, the energy exchanged between small temperature steps might be too low to be correctly monitored by the heat flux sensor compared to the heat flux noise. Temperature steps of 1K are selected in this study as it allows an accurate representation of the thermodynamic state of RT58 while having a short experiment and no influence of the heat flux noise on the measurements. The same heating rate of 0.5 K.min^{-1} than in dynamic mode is set.

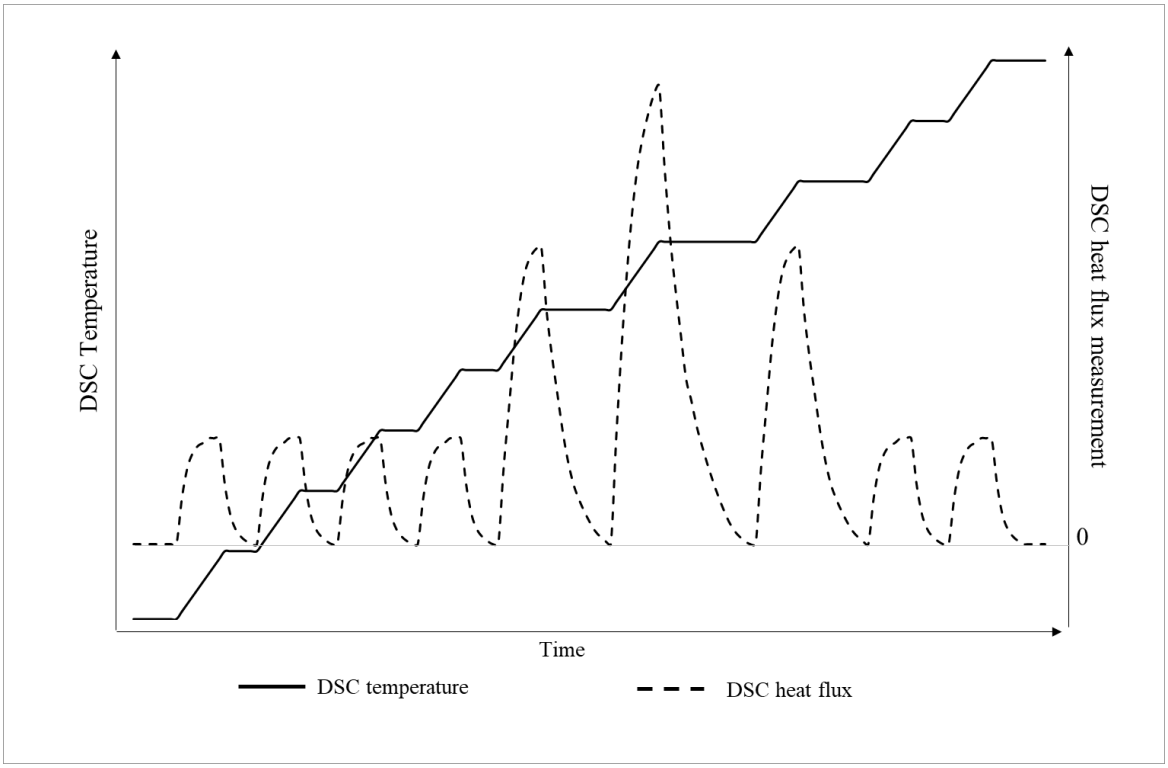

Fig. 2: Principe of DSC characterization with the step mode

3. Inverse method characterizations

3.1. Experimental set-up

The experimental apparatus is a heat flux bench, similar to the one used by (Younsi et al., 2011) and it is detailed in figure 3. The PCM is contained inside a rectangular polymethyl methacrylate (PMMA) brick heated or cooled by two heat exchangers. The PMMA brick measures $210 * 140 * 20$ mm with a wall thickness of 4 mm and contains a mass of 215g of RT58. The heat fluxes and temperatures between the two heat exchangers and the sample are measured by heat fluxmeters on each side of the PMMA brick. The fluxmeters sensitivity is 117 $\mu V.Wm^{-2}$ with an accuracy of 3%. A T-type thermocouple, calibrated at 0.1°C, is also inserted inside the PCM to monitor the variation of the PCM temperature, which is not equivalent to the heat exchangers temperature. The heat transfers within the PCM can be considered in 1D as the lateral sides of the PMMA brick are insulated and the sample width is small compared to the heated surfaces. Heating and cooling ramp of 18h are applied by the heat exchangers to the sample between 20°C and 70°C

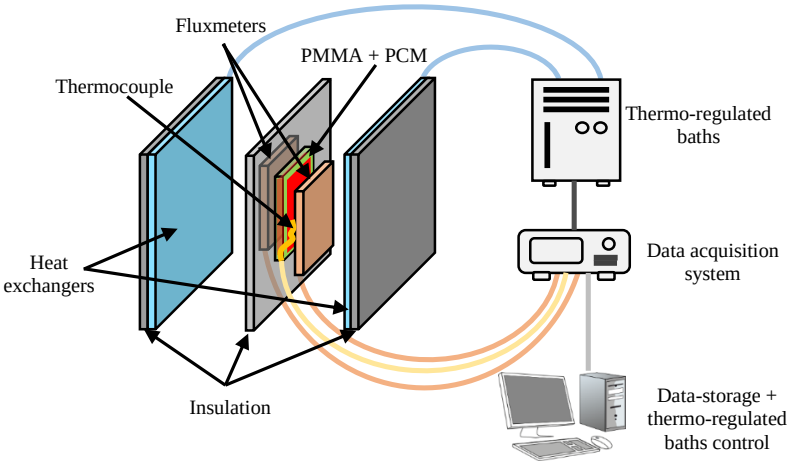

Fig. 3: Experimental apparatus of the heat flux bench

3.2. Modelling of the set-up

The heat flux bench is modelled in 1D by finite difference method with Python programming language. The PCM is discretized in 10 nodes and the boundary conditions of the system are the temperatures applied by the heat exchangers on each side of the sample.

The analytical equation chosen to describe the evolution of the thermodynamic state of the PCM in function of temperature can either be formulated according to the liquid fraction $f(T)$, the effective heat capacity $C_{eff}(T)$ or the enthalpy $H(T)$ as shown with equation 1. Considering only heat transfers by conduction, the equation governing the phase change problem is detailed by equation 2.

$$C_{eff}(T) = \frac{dH(T)}{dT} = Cp_S + (Cp_L - Cp_S) \times f(T) + L \times \frac{df(T)}{dT} \quad \text{(eq. 1)}$$

$$\frac{\partial T}{\partial t} = \frac{\lambda}{\rho\, C_{eff}(T)} \nabla^2 T \quad \text{(eq. 2)}$$

In this study, the analytical model selected describes the evolution of the liquid fraction based on the derivative of an asymmetrical Gaussian function as shown by equation 3. Temperature T_{PC} corresponds to the steepest slope on the liquid fraction curve, which is equivalent to the highest effective heat capacity. Temperature T_S refers to the highest temperature where the PCM is fully solid and temperature T_L to the lowest temperature where the PCM is fully liquid. Coefficients σ_S (equation 4) and σ_L (equation 5) ensure a liquid fraction close to 0 at T_S and to 1 at T_L.

$$f(T) = \begin{cases} \frac{\sigma_S}{\sigma_S + \sigma_L}\left[erf\left(\frac{T - T_{PC}}{\sigma_S}\right) + 1\right] & T \leq T_{PC} \\ \frac{1}{\sigma_S + \sigma_L}\left[\sigma_L \times erf\left(\frac{T - T_{PC}}{\sigma_L}\right) + \sigma_s\right] & T > T_{PC} \end{cases} \quad \text{(eq. 3)}$$

$$\sigma_S = \frac{\sqrt{2}}{4}(T_{PC} - T_S) \quad \text{(eq. 4)}$$

$$\sigma_L = \frac{\sqrt{2}}{4}(T_L - T_{PC}) \quad \text{(eq. 5)}$$

If two heat flux peaks are observed experimentally, equation 1 evolves to equation 6 in order to improve the accuracy of the analytical model. The two heat flux peaks are assumed to be related to two distinct materials, A and B, composing the PCM. The evolution of the liquid fraction of each material, $f_A(T)$ and $f_B(T)$, are supposed independent and the contribution to the total latent heat of the PCM for each material is represented by L_A and L_B. Assuming that specific latent heats of material A and B are equivalent, the total liquid fraction $f_{Tot}(T)$ of the PCM is obtained with a coefficient of latent heat repartition $\epsilon = L_A/(L_A + L_B)$ to weight liquid fraction $f_A(T)$ and $f_B(T)$ by ϵ and $(1 - \epsilon)$, respectively.

$$C_{eff}(T) = Cp_S + (Cp_L - Cp_S) \times f_{Tot}(T) + L_A \times \frac{df_A(T)}{dT} + L_B \times \frac{df_B(T)}{dT} \quad \text{(eq. 6)}$$

3.3. Inverse method principle

The aim of identification by inverse method is to determine unknown parameters involved in the numerical model, such as PCM properties in our case, to fit the numerical results with the experimental ones, which are used as references. The experimental heating and cooling rates are used as input in the numerical model, the output being the numerical heat flux which is compared to the experimental one monitored by the heat fluxmeter sensors. The fitness between the numerical and experimental results is evaluated with the least square approach. Particle swarm optimization (PSO) algorithm is used to perform the inverse method and identify the best set of parameters with the following parametrization: swarmsize=50, particle velocity=0.6, search away particle best known solution=0.7, search away swarm best known solution=0.3.

The main limitation of inverse methods is the convergence as it is not guaranteed that the identified set of parameters is the global solution and not a local solution. The best way to reach convergence is to properly parametrize the optimization algorithm and to reduce the number of parameters to identify.

3.4. Global inverse method

The global identification by inverse method is achieved in three steps. First, the liquid density of the PCM is measured by weighting, right after filling the PMMA brick with the liquid PCM at 70°C. Once fully solid at 20°C, the solid density is obtained by measuring the height difference of the PCM in the PMMA brick compared to liquid state.

The second step consists in performing an inverse method to identify the solid and liquid specific heat capacities and thermal conductivities. Experiments on fully solid and liquid PCM are used as references to identify these parameters.

The third step identifies the latent heat and the parameters involved in the analytical model, to describe the thermodynamic state of the PCM, with a second inverse method. The experiment with heating and cooling ramp of 18h between 20°C and 70°C is selected as reference for the inverse method. Slow heat and cooling ramps make it easier for the PSO algorithm to identify the PCM properties and the phase transition is more distinct than for fast heating and cooling ramps.

3.5. Energy balance inverse method

In the energy balance inverse method, compared to global inverse method, the latent heat and the specific heat capacities of the PCM are identified altogether by energy balance equations on the experimental results. The contribution of sensible heat and latent heat to the total heat flux exchanged by the PCM are presented on figure 4. As shown by equation 7 and equation 8, the solid and liquid specific heat capacities are determined by dividing the sensible heat exchanged on fully solid and liquid state by the temperature range where the PCM is fully solid and liquid respectively. Then, the latent heat (equation 12) is obtained by removing the sensible heats of both the PMMA brick (equation 10) and the PCM (equation 11) to the total heat exchanged by the PCM (Equation 11) during the heating and cooling process. This fourth step, with energy balance identification, is added between step I and II of global inverse method. Then, only the thermal conductivities have to be identified in the first inverse method, and the latent heat is removed to the set of parameters to identify in the second inverse method. Table 1 summarizes the identification process of the global inverse method, detailed in the previous section, and the energy balance method, detailed in this section. Table 2 detailed the PCM properties obtained after performing the global inverse method and the energy balance inverse method.

$$Cp_S = \frac{\left(\sum_{t_0}^{t_1} \phi^{Exp} \times \Delta t\right) - m^{PMMA} \times Cp^{PMMA} \times (T_1^{Hx} - T_0^{Hx})}{m^{PCM}(T_1^{Hx} - T_0^{Hx})} \quad \text{(eq. 7)}$$

$$Cp_L = \frac{\left(\sum_{t_2}^{t_3} \phi^{Exp} \times \Delta t\right) - m^{PMMA} \times Cp^{PMMA} \times (T_3^{Hx} - T_2^{Hx})}{m^{PCM}(T_3^{Hx} - T_2^{Hx})} \quad \text{(eq. 8)}$$

$$E^{Tot} = \sum_{t_0}^{t_3} \phi^{Exp} \times \Delta t \quad \text{(eq. 9)}$$

$$E^{PMMA} = Cp^{PMMA} m^{PMMA} (T_3^{Hx} - T_0^{Hx}) \quad \text{(eq. 10)}$$

$$E^{Sens} = m^{PCM}\left(Cp_S(T_1^{Hx} - T_0^{Hx}) + \frac{Cp_L + Cp_S}{2}(T_2^{Hx} - T_1^{Hx}) + Cp_L(T_3^{Hx} - T_2^{Hx})\right) \quad \text{(eq. 11)}$$

$$L = \frac{E^{Tot} - E^{PMMA} - E^{Sens}}{m^{PCM}} \quad \text{(eq. 12)}$$

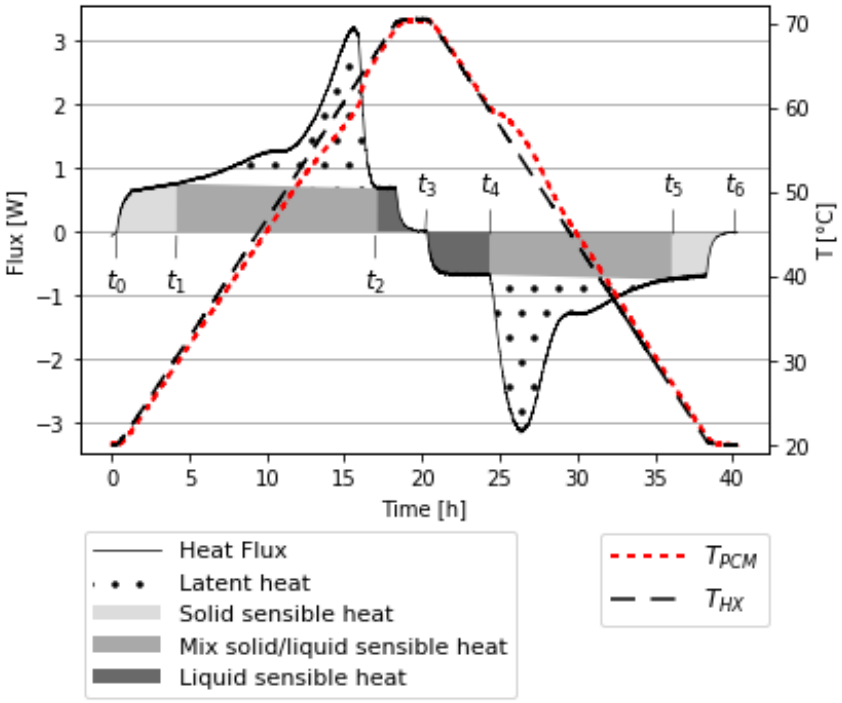

Fig. 4: Contribution of sensible heat and latent heat to the total heat exchanged by the PCM

Tab. 1: Identification process of PCM properties for global inverse method and energy balance inverse method

PCM properties	Global inverse method	Energy balance inverse method
ρ_S, ρ_L	Experimental weighting (step I)	Experimental weighting (step I)
Cp_S, Cp_L	Inverse Method I (step II)	Energy balance (step II)
λ_S, λ_L	Inverse Method I (step II)	Inverse Method I (step III)
L	Inverse Method II (step III)	Energy balance (step II)
$\epsilon, T_{S\,A}, T_{PC\,A}, T_{L\,A}, T_{S\,B}, T_{PC\,B}, T_{L\,B}$	Inverse Method II (step III)	Inverse Method II (step IV)

Adding a fourth step to the identification process present two main advantages. First, it ensures an equivalent energy balance between the experimental and numerical results as the specific heat capacities and the latent heat are identified directly on experimental results. Secondly, fewer parameters have to be identified on inverse method I and II, which means a faster optimization time to converge to the global solution.

4. Results

Before comparing results from DSC experiments and inverse methods, the accuracy of the global inverse method and the energy balance inverse method has to be checked. As shown by figure 5 and figure 6, both global inverse method and energy balance inverse method represent correctly the evolution of the temperature and the heat flux, the main heat flux peak being around 59°C and the secondary one around 45°C. The selected analytical model combined to the modelling of two materials A and B is then relevant to model paraffin RT58. The difference between the two methods seems minimal but, when having a closer look at the evolution of the error between numerical and experimental results with figure 7, a slightly better accuracy is observed for the global inverse method. This was expected as the latent heat is identified with the global inverse method to fit the experimental and numerical heat flux curves, and then perform better than for the energy balance inverse method where the latent heat is fixed by experimental results.

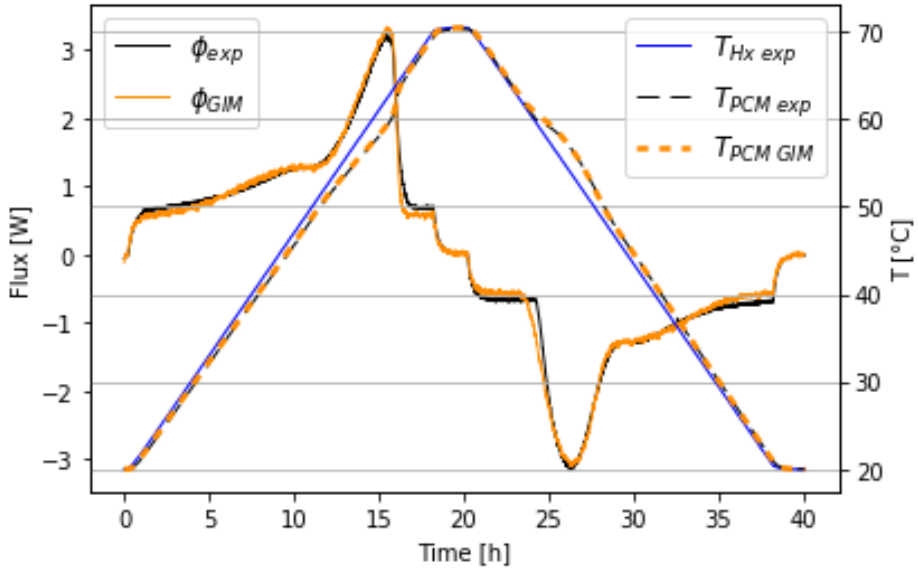

Fig. 5: Comparison between experimental and numerical heat flux and temperature for the global inverse method (GIM)

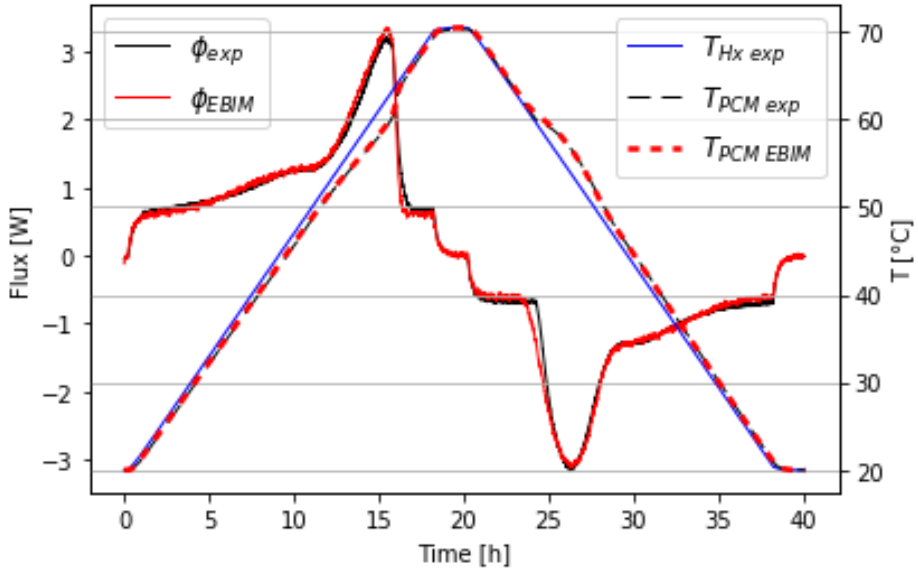

Fig. 6: Comparison between experimental and numerical heat flux and temperature for the energy balance inverse method (EBIM)

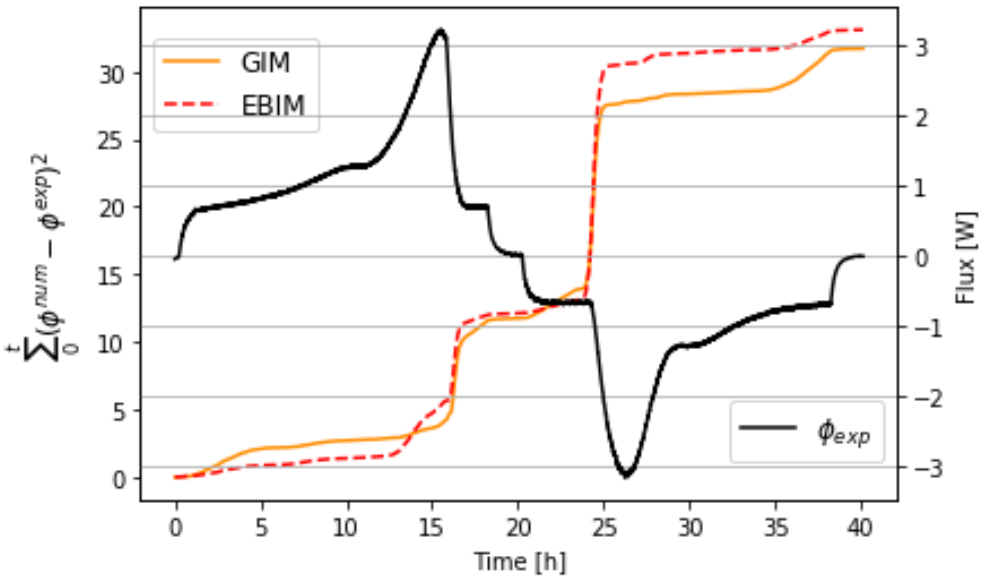

Fig. 7: Evolution of the quadratic error between experimental and numerical heat flux for the global inverse method (GIM) and the energy balance inverse method (EBIM)

The enthalpy curves obtained with each method are presented figure 8. All four characterization methods lead to almost the same enthalpy curve in overall. The final enthalpy value only differs by 3.3% between the highest one, the energy balance inverse method, and the lowest one, the DSC dynamic mode. The scale difference between the DSC sample and the brick sample used in the heat flux bench does not influence the enthalpy curve. The results from DSC dynamic mode are almost equivalent than those from step mode, implying that heating and cooling rate of 0.5 $K.min^{-1}$ is appropriate for the characterization of RT58. As shown by table 2, differences between PCM properties identified by the two inverse methods are minimal and therefore leads to an almost equivalent enthalpy curve. Eventually, each method seems appropriate to identify the enthalpy curve or RT58. The modelling of complete melting and solidification will hardly change from one method to another.

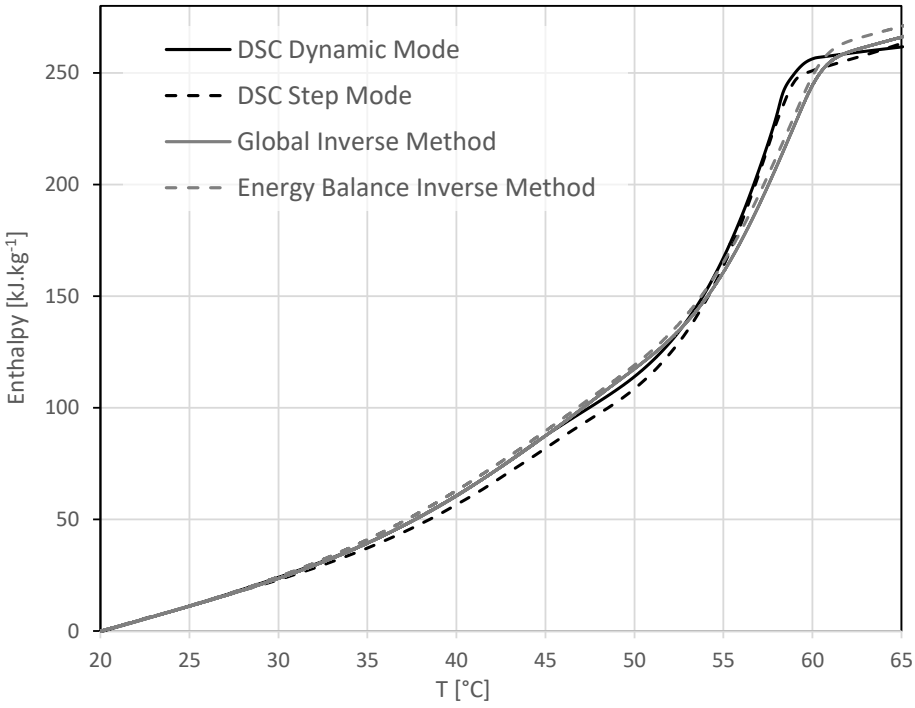

Fig. 8: Enthalpy curve of paraffin RT58 obtained with the four characterization methods tested (from reference set at zero at 20°C)

Tab. 2: PCM properties identified with global inverse method (GIM) and energy balance inverse method (EBIM)

PCM properties	Unit	GIM	EBIM
ρ_S	$kg.m^{-3}$	880	880
ρ_L	$kg.m^{-3}$	808	808
Cp_S	$J.kg^{-1}.K^{-1}$	1925	2112
Cp_L	$J.kg^{-1}.K^{-1}$	1975	2100
λ_S	$W.m^{-1}.K^{-1}$	0.198	0.206
λ_L	$W.m^{-1}.K^{-1}$	0.241	0.237
L	$kJ.kg^{-1}$	177.2	172.4
ϵ	-	0.32	0.30
$T_{S\,A}$	°C	10.0	9.7
$T_{PC\,A}$	°C	45.4	45.4
$T_{L\,A}$	°C	60.2	59.8.
$T_{S\,B}$	°C	40.6	39.6
$T_{PC\,B}$	°C	59.3	59.3
$T_{L\,B}$	°C	63.6	63.7

However, small differences still exist between the different characterization methods, especially between DSC and inverse methods. Indeed, the two DSC methods and the two inverse methods give a slightly different evaluation of the end of the phase change process. The liquid state seems to be fully reached at 59.5°C for the two inverse methods and at 60.5°C for the DSC methods. It results in a maximal enthalpy difference of 25 $kJ.kg^{-1}$ at 59°C, which might lead to different numerical performances, particularly for partial phase change around 57-60°C.

5. Conclusion

To conclude, four characterization methods have been tested to determine the enthalpy curve of RT58, two based on DSC methods with dynamic mode and step mode, the other two relying on a numerical model to identify the PCM properties with a global inverse method or an energy balance inverse method. Results are mainly similar for each method with an equivalent heat exchanged. The phase change dynamic on the phase change temperature range is however slightly different between the two DSC methods and the two inverse methods. Modelling of complete phase change will be almost not influenced, but the modelling of partial phase change might be slightly different. The equivalence between the four characterization methods is only relevant for the considered PCM RT58 and cannot be withdrawn to other PCM.

6. Acknowledgments

This study takes part in the EUROPA project funded by the ANR (French National Research Agency).

7. References

Dolado, P., Mazo, J., Lázaro, A., Marín, J.M., Zalba, B., 2012. Experimental validation of a theoretical model: Uncertainty propagation analysis to a PCM-air thermal energy storage unit. Energy and Buildings 45, 124–131. https://doi.org/10.1016/j.enbuild.2011.10.055

Dumas, J.-P., Gibout, S., Zalewski, L., Johannes, K., Franquet, E., Lassue, S., Bédécarrats, J.-P., Tittelein, P., Kuznik, F., 2014. Interpretation of calorimetry experiments to characterise phase change materials. International Journal of Thermal Sciences 78, 48–55. https://doi.org/10.1016/j.ijthermalsci.2013.11.014

Franquet, E., Gibout, S., Bédécarrats, J.-P., Haillot, D., Dumas, J.-P., 2012. Inverse method for the identification of the enthalpy of phase change materials from calorimetry experiments. Thermochimica Acta 546, 61–80. https://doi.org/10.1016/j.tca.2012.07.015

Gibout, S., Molina, S., Haillot, D., Franquet, E., 2017. Méthode STEP : Caractérisation de La Précision et Conditions Optimales d'analyse. In XIIIe Colloque interuniversitaire franco-québécois sur la Thermique des Systèmes énergétiques (CIFQ).

Lazaro, A., Peñalosa, C., Solé, A., Diarce, G., Haussmann, T., Fois, M., Zalba, B., Gshwander, S., Cabeza, L.F., 2013. Intercomparative tests on phase change materials characterisation with differential scanning calorimeter. Applied Energy 109, 415–420. https://doi.org/10.1016/j.apenergy.2012.11.045

Sharma, A., Tyagi, V.V., Chen, C.R., Buddhi, D., 2009. Review on thermal energy storage with phase change materials and applications. Renewable and Sustainable Energy Reviews 13, 318–345. https://doi.org/10.1016/j.rser.2007.10.005

Tittelein, P., Gibout, S., Franquet, E., Zalewski, L., Defer, D., 2015. Identification of Thermal Properties and Thermodynamic Model for a Cement Mortar Containing PCM by Using Inverse Method. Energy Procedia 78, 1696–1701. https://doi.org/10.1016/j.egypro.2015.11.265

Younsi, Z., Zalewski, L., Lassue, S., Rousse, D.R., Joulin, A., 2011. A Novel Technique for Experimental Thermophysical Characterization of Phase-Change Materials. International Journal of Thermophysics 32, 674–692. https://doi.org/10.1007/s10765-010-0900-z